FRACTURE ANALYSIS IN 5HS CARBON COMPOSITES SUBJECTED TO PURE MODES I AND II FATIGUE INDUCED DELAMINATION

M. Y. Shiino[a*], R. C. Alderliesten[b], M. V. Donadon[c], M. Y. Pitanga[a], M. O. H. Cioffi[a]

[a]*Guaratinguetá Faculty of Engineering, UNESP - Univ Estadual Paulista , Materials and Technology Department, Fatigue and Aeronautic Materials Research Group, 333, Dr. Ariberto Pereira da Cunha Ave., 12516-410, Guaratinguetá- SP, Brazil, marcosshiino@yahoo.com.br*
(Times New Roman 11pt, Italic, left-aligned)
[b]*Faculty of Aerospace Engineering, TUDelft – Delft University of Technology, Structural Integrity & Composites, Kluyverweg 1, 2600 GB, Delft, The Netherlands*
[c]*Instituto Tecnológico da Aeronáutica, S.J.Campos/SP, Brazil, Praça Marechal do Ar Eduardo Gomes, Vila das Acacias CEP 12228-900 São José dos Campos/SP, Brazil*

Keywords: Laminate; Fatigue; Fractography.

Abstract
Interlaminar fracture process in woven composite laminate in general takes place in a nonlinear front propagation when analyzing a 2-D propagation for mode I opening. The nonlinearity is justified by the arresting crack at the warp yarn. Regarding mode II opening, the crack interaction to the crimp surface still needs further assessment. The tortuous crack path and, consequently, loading directions on both modes were determined in this work by fractographic analysis of quasi-static and cyclic loading fractured in 5HS carbon/epoxy composite specimens. The crack growth rate and strain energy release rate were compared to the fractographic images that approximately pointed out the driving force in each delamination stage. Mode I fracture surface showed to have more influence on fracture toughness (G_{Ic}) than amplitude loading while mode II fracture surface suggested the opposite behavior, all based on the well-known fracture patterns established along the years for other composite architectures.

1. Introduction

Woven fabrics employed in laminate composites have been widely applied in engineering structures due to their good characteristic of drapability and high damage tolerance [1]. Other remarkable characteristic of woven fabrics is the enhanced delamination resistance compared to unidirectional tapes, but has reduced compressive strength because of the crimp produced by the interlacing tows [2].

Interlaminar fracture toughness (G_{IC}) in composites is determined by the strain energy release rate (SERR) based on Griffith theory being a more suitable way to deal with a non homogeneous structure of fiber and matrix compositions [3,4]. By taking the parameter G into account to describe crack propagation, it was reported that the crack path varied according to the type of fabric, normally presenting a start-stop behavior that reflects in a serrated profile of $G_I \times a$ in R-curve [5].

For mode II the propagation under quasi-static condition is more unstable as compared to mode I. For example in multidirectional laminates it was reported crack jump and crack formation ahead of the main crack or in neighboring layers [6,7].

The micromechanisms that describe the crack path in unidirectional laminates can be distinguished for modes I and II by analyzing the fractographic images, but for other fiber architectures it can involve both modes of loading even testing for only one mode. Greenhalgh et al. [8] presented evolution of fracture micromechanisms from pure mode I changing to a mix mode until reaches pure mode II. Mode I loading exhibits clean surface that indicates matrix cleavage, fracture process which characteristically indicates low energy dissipated in the fracture process. Some related fracture patterns in ply separation process usually are feather, river marks, scarps, and ribbons [9]. By increasing mode II component, a rougher surface is created following an increasing energy necessary to create a new delamination. The resulting fracture pattern for pure mode II loading is represented by cusps makings that also appears in mix mode in multidirectional laminates [8,9,10]. According to Greenhalgh et al. [8] the high energy (G_{IIc}) in mode II is attributed to a fractured area around the crack tip and is derived locally by G_{Ic}.

In regard to fracture surface in fatigue tests, few works reported the patterns of fractured surface in more complex fiber architecture. In work conducted by Shiino et al.[10] it showed the cusps size dependence on a number of cyclic loads in quasi-isotropic laminate under uniaxial load as shown in Fig 1. On the other hand, in a more general way, Gilchrist et al. [11] stated that no fatigue life can be determined by using cusp parameter, due to the fretting and abrasion process that obscures any fracture pattern. Otherwise the latter author mentioned striation as an important fatigue fracture pattern for tough epoxy system, as a similar feature to fracture surface in metals. For pure mode I and II Gilchrist et al. [11] did not find any difference between static and cyclic loading fracture surface.

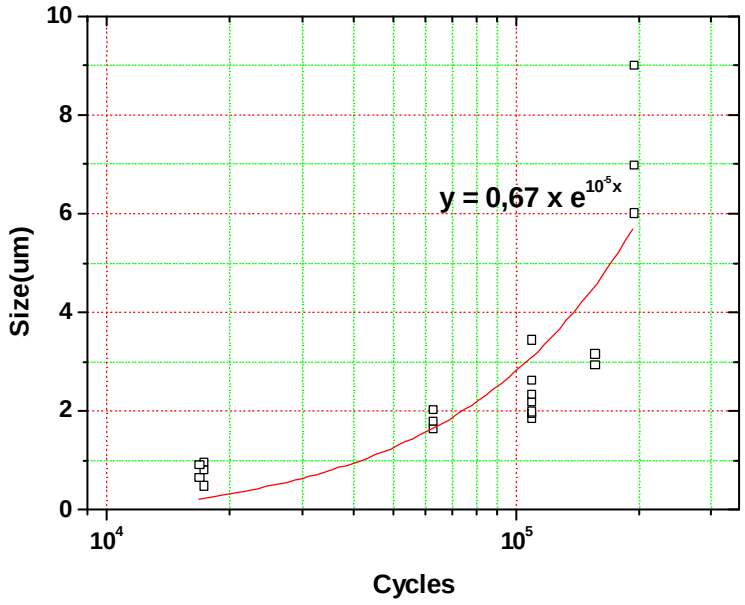

Figure 1. Variation of cusp size with fatigue life in multidirectional composite adapted from [10].

Considering the importance of fracture surface and the type of load that generated the failure, it was conducted fractographic investigation to cover that lack of information with respect of fracture surface under cyclic load with different crack growth rate. The fractured surfaces

obtained in double cantilever beam (DCB) and end-notch-flexure (ENF) specimens were firstly observed in optical microscopic and further conducted a detailed analysis in Scanning Electron Microscopy (SEM).

2. Materials and Methods

2.1. Specimen preparation and fatigue test

The laminate plate was processed with a RTM-6 bicomponent resin system, with viscosity 100 mPa.s at 80°C approximately for the injection cycle. For cure cycle, the temperature was risen at a ratio of 5 °C/min until reached 180°C for 120 minutes.

The 5HS woven carbon fabric with areal weight of 391 g/m^2 and fiber tow of 6K was preformed prior to the injection, this process was possible due to the epoxy powder in both fabric surfaces. The preform comprising 8 layers resulted in a laminate with 58% of fiber volume fraction in a 3 mm thickness cavity. In the middle of the perform it was placed a 13 μm PTFE insert film in the laminate edge to produce an artificial pre-crack as specified in standard test method [12].

The fatigue test was conducted in a 5 kN MTS testing machine that cyclic loaded the specimen arms with a frequency of 5 Hz, a stress ratio of R=0.1, and using displacement control in both opening modes. The combination of maximum (δ_{max}) and constant displacement assured the data acquisition for decreasing values of *da/dN* ratios and, consequently, ΔG energy.

The data reduction to calculate the energy release rate followed the derivation of *dC/da* function of the Irwin-Kies equation, Eq. (1), in which the equation of the compliance change as a function of the crack increment can be calculate according to Eq. (2).

$$G = \frac{P^2}{2B}\frac{dC}{da} \tag{1}$$

$$C = ma^n \tag{2}$$

Where *m* and *n* are parameters to be experimentally determined by fitting the logarithm of *C* and *a* in a double *Log* curve.

For the mode II, similar test specimen were used but this time with a three-point-bending device. A support span was employed equal to 2L=100 mm, an initial crack length equal to a_0=35mm. The method is based on compliance based beam method (CBBM) that depends on the corrected coupon compliance, the equations and procedures for data reduction are well outlined in work conducted by Moura et al. [13].

The driving force considered in this work for damage propagation is related to the applied cyclic loads and for similarity condition it was adopted $\Delta G = G_{eff}$ defined by the superposition rule as $(\sqrt{G_{max}} - \sqrt{G_{min}})^2$ that direct relates to the amplitude load range ΔP [14].

2.2. Fractographic investigation

The first analysis was conducted at fractured open edge that was careful polished according to the following condition of material and parameter (sand paper number/rotation/time in minutes) and the sequence: (400/200/4); (600/250/4); (1200/300/5); (1 μm diamond particles/300/6) and (0.25 μm silica colloidal solution/350/6). In every step the specimens were cleaned in an ultrasonic bath for 2 minutes. Afterwards the edge was observed in an optical microscopy in bright field and reflection technique in order to distinguish carbon fiber from epoxy matrix.

The Scanning Electron Microscopy was performed using a JEOL-JSM5310 equipment with a tungsten filament working at 15 keV. The electron beam of 15 keV was the most suitable choice for the studied material providing a detailed topographic information. A gold thin layer coated the fractured specimens in order to increase the electron conductivity. A film with less than 20 nm is recommended to avoid any interference in the topographic information.

3. Results and discussions

Fig. 2a shows the crack propagation at high G_I that did not introduce damage into the tow as at this point the propagation can be compared to quasi-static G_{Ic}. Meanwhile at half-way of the da/dN curve showed in Fig. 3, a damage zone around the crack tip was introduced prior to the crack propagation as indicated by the arrow in Fig.2b. In mode I case the damage usually crossed the weft tows, weft is considered here as perpendicular to the crack propagation direction.

Mode II propagation initiated at 72% of G_{IIc} facing warp/warp interface as shown in Fig.2c. For any range of G_{eff} the crack was located in the same interface thus it did not crossed weft tow as observed for mode I. Important to note a damage zone for mode II however at the same interface instead of affecting a region around the crack tip as occurred for mode I as showed the linear crack path in Fig. 2c and 2d.

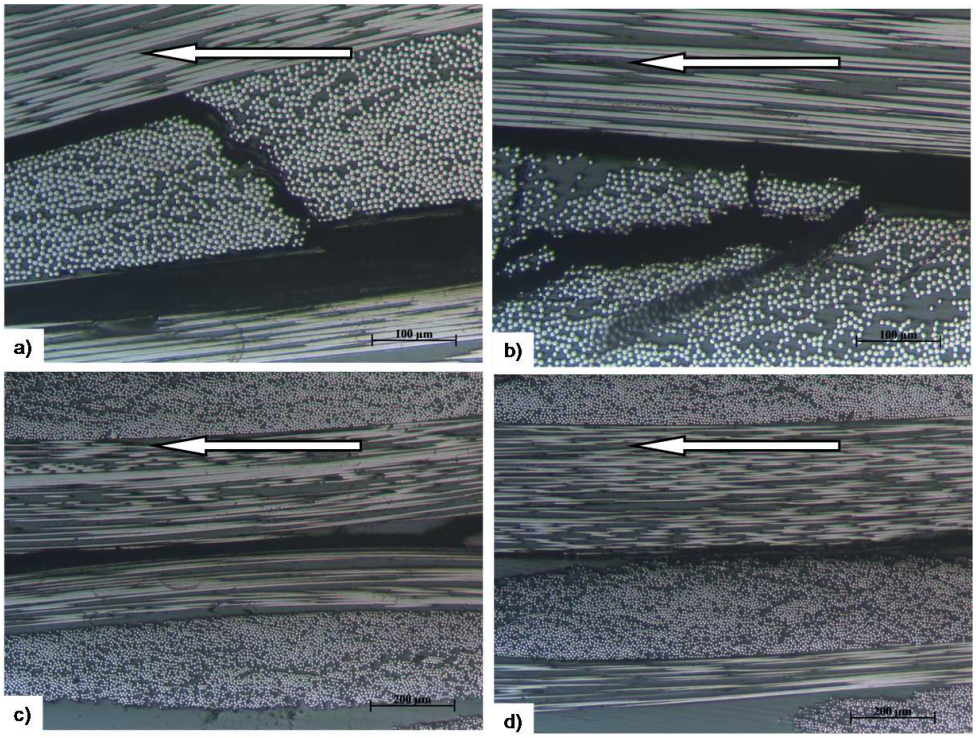

Figure 2. Crack path along the edge: a) at the crack tip, mode I; b) at $2x10^{-3}$ mm/cycle growth rate in mode I; c) at the crack tip, mode II; d) at $1x10^{-4}$ mm/cycle growth rate in mode II.

In both modes the crack propagation rate changed to a region that did not follow a Paris law due to the arresting crack in regions at the weft section. This phenomena is more evident in mode I in the 200 to 240 J/m^2 range as showed in Fig. 3a. Rectangular details indicated by the areas in Fig.3b are related to threshold regions and with unstable fast crack growth rate. Between these two regions a fairly linear behavior in terms of *Log(da/dN)* versus *Log(G_{eff})* was observed. A detailed investigation on micromechanisms of fracture for this region is described in the next paragraphs.

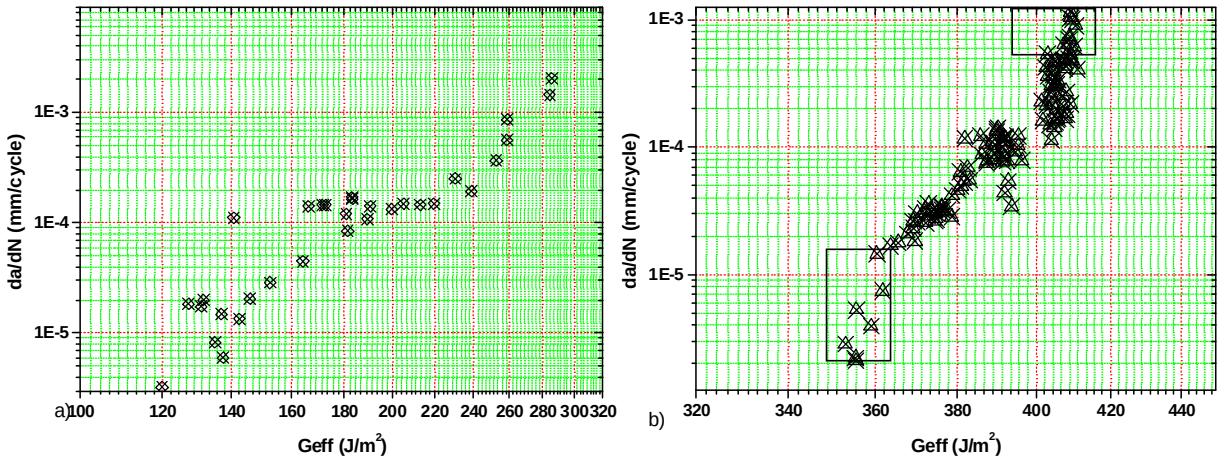

Figure 3. Crack propagation rate: a) mode I; b) mode II obtained by equivalent crack method.(ECM).

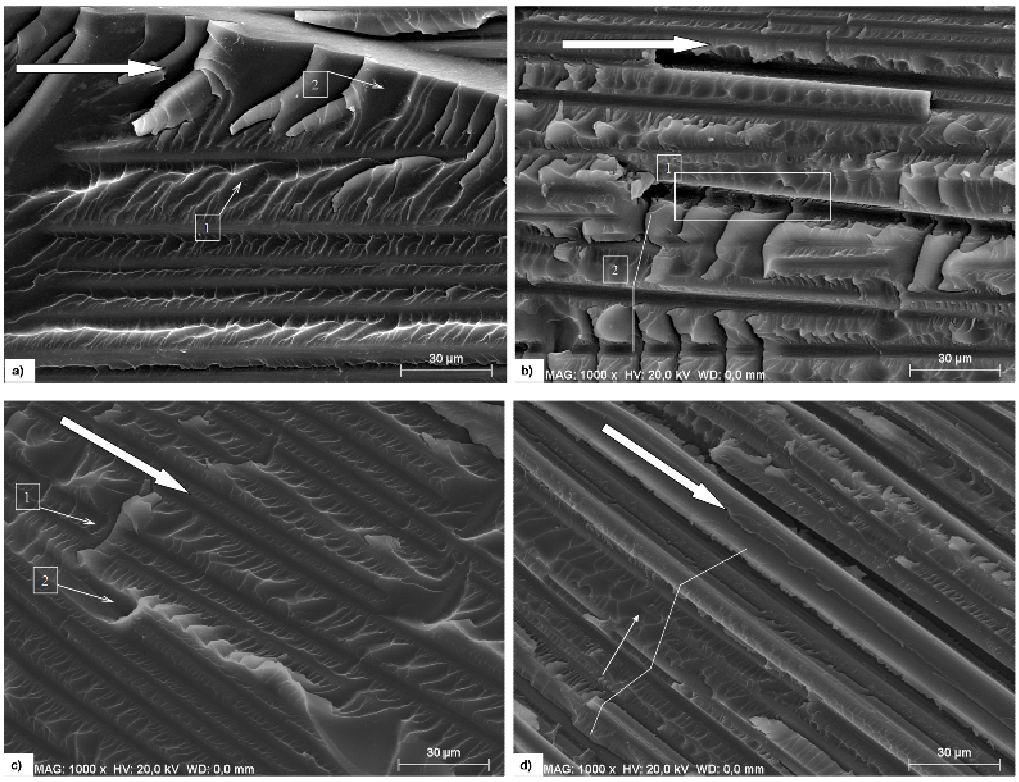

Figure 4. Fracture surface: a) mode I at fast propagation; b) mode I at approximately $1.5x10^{-4}$ mm/cycle; c) mode I at approximately $4.5x10^{-5}$ mm/cycle; c) mode I at approximately $8x10^{-6}$ mm/cycle.

In all Figures the full arrows indicate the global propagation and the small ones followed by numbers indicate a local propagation. In Fig.4a detail 1 shows the formation of scarps between the fiber tows and at the tip of this pattern may indicate the end of the fracture process. On the top of Fig.4a detail 2, it is shown the formation of cusps due to an overload and oblique direction of referred load.

Fig. 4b shows a typical fracture surface associated with the region of constant crack growth (between 200 to 240 J/m^2). Detail 1 indicates the peeling process with a missing fiber and also detail 2 shows the mirror of the ribs that also demonstrates the same tensile stress, as reported by Purslow [9]. Fig 4c shows the same micromechanisms from the previous one but with less matching ribs. Moving to a region close to a threshold region in Fig.4d, the scarps seem less sharp and the crack crossed into the warp tow (intratow-showed by small arrow) in different planes thus causing more damage than other sections.

Further analysis was conducted at the center of the fractured specimen following the same sequence of the previous paragraph described in Fig. 4. Images captured in this region presented featureless patterns compared to that taken from the edge as seen in Fig.5a and 5b. These regions encompass the low propagation rate in which the dashed line demonstrates the smooth transition that could relate the influence of the amplitude loading as formulated using superposition rule.

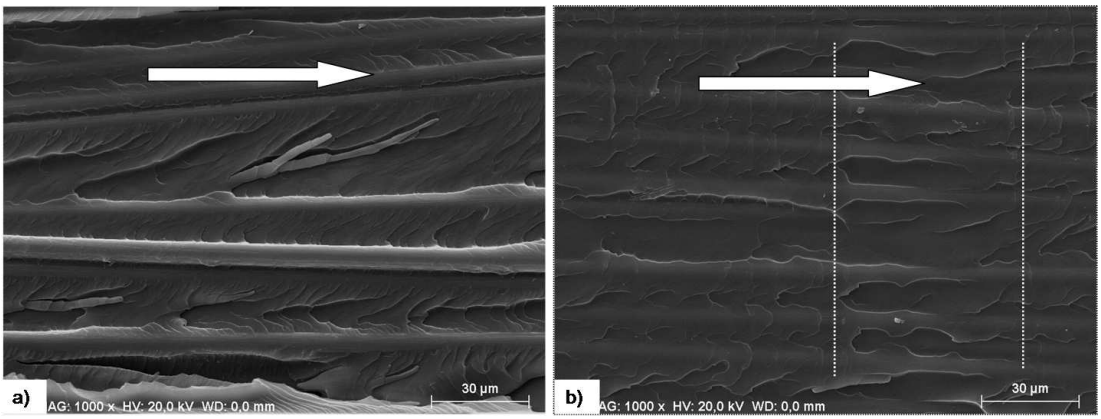

Figure 5. Fracture surface: a) mode I at approximately 1.5x10^{-4} mm/cycle; b) mode I at approximately 1.8x10^{-5} mm/cycle.

The mode of failure has meaningful difference between fractographs achieved from the edge and from the center, the former presenting more fiber/matrix interfacial failure while at the center more cohesive failure, both regions under cyclic loadings. According to Greenhalgh [2], cohesive failure is related to quasi-static failure in the meanwhile the smooth surface in Fig. 5b is also related to fatigue failure.

Fractographs were taken only at the warp section as at the weft section the tows hold all the peel loading and after damaging this section the propagation takes place in a quasi-static manner without any feature of fatigue loadings along it.

Mode II fracture surface of static and fatigue specimen can be differentiated by means of cusp and roller formation, respectively [2]. Most of the analysis was conducted in the warp section, in which mode II propagation showed the roller formation with increasing debris when moving towards the delamination length which is related to the reduced crack propagation rate as seen in Fig 6.

The roller formation provides evidences of decreasing amplitude loading acting on the fracture surface as a consequence of increasing number of cyclic loads in this area. This can be distinguished, at this point, from the debris of detached rollers rather than the fracture surface as this characteristic feature could depend on the matrix content between fibers.

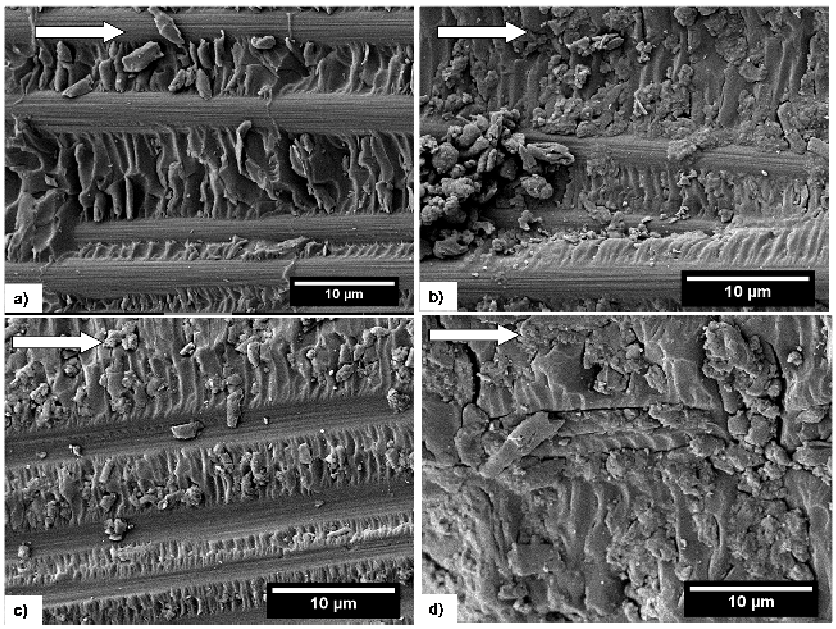

Figure 6. Fracture surface: a) mode II at 72%G_{IIc}; b) mode II at approximately $4x10^{-4}$ mm/cycle; c) mode II at approximately $4x10^{-5}$ mm/cycle; b) mode II at approximately $4x10^{-6}$ mm/cycle.

In the weft section, very poor information was left on the fracture surface. Nonetheless striation, as defined in [2] can be found in resin rich regions as detailed in Fig.7. Note that it resembles to feather patterns [9], however it has a nucleation point that propagated in the same direction of the global delamination.

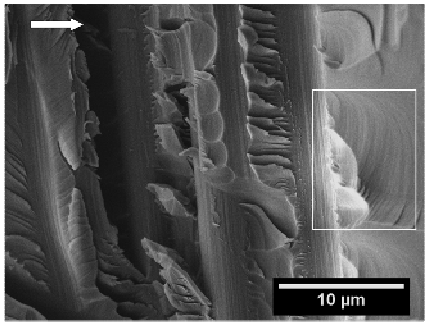

Figure 7. Fracture surface at the weft section.

4. Conclusions

This paper explained how the driving force, adopted as G_{eff} , acted to produce the fracture patterns in mode I and II by knowing the global propagation direction. So far the fracture surface on mode I had few characteristic features that links to the amplitude loading despite the cohesive failures showed in the discussion section. In this fiber architecture more interference of the weft tows can hide the studied characteristics of cyclic loadings.

For mode II the aforementioned interference had less influence in the warp section, as seen in linear part of Paris law in Fig.3b, as in this mode an area is involved in the crack propagation thus delaminating in a linear path. Then the adopted law that related the similitude of stress intensity factor (ΔK) is suitable for mode II.

Acknowledgements

The authors acknowledge the financial support received from FAPESP contract number 2011/01937-0.

References

[1] T. Lisle, C. Bouvet, M.L. Pastor, P. Margueres, R.P. Corral. Damage evaluation in a thin woven composite laminate under static tension using infrared thermography. Composites: Part A 53:75-87A, 2013.
[2] E.S. Greenhalgh. Failure analysis and fractography of polymer composites. CRC Press, Cambridge, 2009.
[3] M. Kenane, Z. Azari, S. Benmedakhene, M.L. Benzeggagh. Experimental development of fatigue delamination threshold criterion. Composites Part B: engineering 42:367-375, 2011.
[4] V.A. Pastoukhov, H.J.C Voorwald. Introdução à mecânica da integridade estrutural. Editora UNESP, São Paulo, 1996.
[5] T. Ebeling, A. Hiltner, E. Baer, I.M. Fraser, M.L. Orton. Delamination failure of woven glass fiber composite. Journal of Composite Materials 31:1318-1333, 1997.
[6] A.B. Morais. Analysis of mode I interlaminar fracture of multidirectional laminates. Composites Part A: applied science and manufacturing 35:51-57, 2004.
[7] R.H. Martin. Interlaminar fracture characterization. Key Engineering Materials 120-121: 329-346, 1996.
[8] E. S. Grenhalgh, C. Rogers, P. Robinson. Fractographic observations on delamination growth and subsequent migration through the laminate. Composite Science and Technology. 69:2345-2351, 2009.
[9] D. Purslow. Matrix fractography of fibre-reinforced epoxy composites. Composites. 17:289-303, 1986.
[10] M.Y. Shiino, L.M. Camargo, M.O,H. Cioffi, H.J.C. Voorwald, E.C. Ortiz, M.C. Rezende. Correlation of microcrack fracture size with fatigue cycling on non-crimp fabric/RTM6 composite in the uniaxial fatigue test. Composites Part B: engineering 43:2244-2248, 2012.
[11] M.D. Gilchrist, N. Svensson. A fractographic analysis of delamination within multidirectional carbon/epoxy laminates. Composites Science and Technology. 55:195-207, 1995.
[12] ASTM D 5528-01, Standard Test Method for Mode I Interlaminar Fracture Toughness of Unidirectional Fiber-Reinforced Polymer Matrix Composites.
[13] M.F.S.F. Moura, R.D.S.G. Campilho, J.P.M. Goncalvez. Pure mode II fracture characterization of composite bonded joints. International Journal of Solids and Structures. 46:1589-1595, 2009.
[14] C.D. Rans, R.C. Alderliesten, R. Benedictus. Misinterpreting the results: how similitude can improve our understanding of fatigue delamination growth. Composites Science and Technology. 71:230-238, 2011.